HHS Public Access

Author manuscript

Chem Mater. Author manuscript; available in PMC 2016 January 01.

Published in final edited form as:

Chem Mater. 2015 ; 27(16): 5668–5677. doi:10.1021/acs.chemmater.5b02086.

Super stretchable electroactive elastomer formation driven by aniline trimer self-assembly

Jing Chen[a], **Baolin Guo**[a], **Thomas W. Eyster**[b], and **Peter X. Ma**[a,b,c,d,e,*]

[a]Center for Biomedical Engineering and Regenerative Medicine, Frontier Institute of Science and Technology, Xi'an Jiaotong University, Xi'an, 710049, China

[b]Department of Biologic and Materials Sciences, University of Michigan, Ann Arbor, MI 48109, USA

[c]Department of Biomedical Engineering, University of Michigan, Ann Arbor, MI 48109, USA

[d]Macromolecular Science and Engineering Center, University of Michigan, Ann Arbor, MI 48109, USA

[e]Department of Materials Science and Engineering, University of Michigan, Ann Arbor, MI 48109, USA

Abstract

Biomedical electroactive elastomers with a modulus similar to that of soft tissues are highly desirable for muscle, nerve, and other soft tissue replacement or regeneration, but have rarely been reported. In this work, superiorly stretchable electroactive polyurethane-urea elastomers were designed based on poly(lactide), poly(ethylene glycol), and aniline trimer (AT). A strain at break higher than 1600% and a modulus close to soft tissues was achieved from these copolymers. The mechanisms of super stretchability of the copolymer were systematically investigated. Crystallinity, chemical cross-linking, ionic cross-linking and hard domain formation were examined using differential scanning calorimetry (DSC), X-ray photoelectron spectroscopy (XPS), dynamic light scattering (DLS), nuclear magnetic resonance (NMR) measurements and transmission electron microscopy (TEM). The sphere-like hard domains self-assembled from AT segments were found to provide the crucial physical interactions needed for the novel super elastic material formation. These super stretchable copolymers were blended with conductive fillers such as polyaniline nanofibers and nanosized carbon black to achieve a high electric conductivity of 0.1 S/cm while maintaining an excellent stretchability and a modulus similar to that of soft tissues (lower than 10 MPa).

*Corresponding Author: (P.X.M) – mapx@umich.edu.

Supporting Information

Materials, experimental details, and characterization data: List of materials and their sources; FTIR characterization of PEG2K, AT, PLLA, and of PEG2k-AT6-TMP; NMR characterization of PEG2k-AT6-P; gel permeation chromatography of copolymers; UV-visible spectra of PEG2k-AT6-P in THF and DMSO; cyclic voltammogram curve generation for copolymers; copolymer melting temperature measurements by differential scanning calorimetry; tensile strength, breaking elongation, and Young's modulus measurements of copolymers via tensile testing; dynamic light scattering measurements of copolymer aggregates; x-ray photoelectron spectroscopy of PEG2k-AT6-TMP and PEG2K-AT6-nD-TMP; FT-IR spectra of networks with varied PEG segments; transmission electron microscopy of PEG2k-AT6-P, 2% polyaniline nanofibers, 2% polyaniline nanofibers/PEG2k-AT6-P blend film, and 2% carbon black/PEG2k-AT6-P blend films. This material is available free of charge via the Internet at http://pubs.acs.org.

Introduction

Elastomeric biomaterials are highly desired in a variety of biomedical applications.[1] Synthetic biomedical elastomers such as poly(glycerol sebacate), poly(1,8-octanediol-citrate), poly(ether ester), polyurethane and polylactide block copolymers have received tremendous attention because of their elastomeric properties, which mimic the mechanical behavior of certain soft tissues.[2]

Polyurethane (PU) elastomers in particular show great promise due to the tunability of their mechanical properties via varying the chemical compositions of their hard and soft segments. While PU elastomers have been explored as biomaterials for blood vessel, heart valve, nerve, and articular cartilage repair or regeneration,[3–4] most of the PU elastomers studied thus far have a relatively low strain at break.[5–8] While the maximum elongation of several PU/poly(caprolactone) (PCL) copolymers can reach values greater than 1000%,[9–10] the Young's modulus of PCL-based PU materials is higher than 20 MPa, significantly stiffer than soft tissues such as smooth muscle and nerve (possessing a modulus lower than 10 MPa).[2, 11–12] Macroscopic mimicry of soft tissues is critically important for next generation biomaterials – for example hydrogels and 3D scaffolds have been developed which display some soft tissue properties.[13–15] While many materials have been developed to mimic hard tissues such as bone, true soft tissue-mimicking mechanical properties have not been achieved from a PU elastomer for vascular or nerve tissue engineering.[16–17]

Electroactive materials have been developed for actuators,[18–19] organic sensors,[20–21] and artificial muscles.[22–23] Electroactive biomaterials could also be advantageous since many types of cells, including neurons and muscle cells, respond to electrical stimulations.[24–26] Polyaniline (PANI) is a promising conductive polymer because of its electrical conductivity and its unique oxidation and reduction transition chemistry.[27–29] As analogues to PANI, aniline oligomers have received increasing attention recently due to their electroconductivity and superior solubility/processability compared to PANI. In addition, biomaterials based on aniline trimer (AT),[30–31] aniline tetramer,[32] and aniline pentamer[32–33] have been explored on account of their low cytotoxicity. Moreover, aniline oligomers can self-assemble into stable nano-/micro-structures because of their well-defined molecular structure.[34–35] Nevertheless, oligoaniline-based elastomers have rarely been reported.

We aim to design an AT-based electroconductive elastomer with a high stretchability and low modulus similar to those of soft human tissues. We hypothesize that when incorporated into PU's hard segment, AT's rigid aromatic structure would enable strong π-π stacking interactions and facilitate the formation of hard domains as advantageous physical cross-links. By achieving a uniform distribution of hard domains in a network of long soft chains, we aim to develop the desired mechanical properties (super stretchability and low modulus). A series of copolymers were therefore synthesized using AT as the hard block and FDA approved poly(L-lactide) (PLLA, M_n=1500) and poly(ethylene glycol) (PEG) as the soft blocks - providing biodegradability and hydrophilicity, respectively. Excitingly, exceptionally high stretchability (larger than 1600%) and a desirable low modulus (less than 10 MP) were achieved for soft tissue engineering applications. Moreover, various compositions were designed to examine the effect of AT content and other factors (such as

crystallinity and ionic interactions) on mechanical properties of the copolymers. Based on careful analysis of data, several models of contributing interactions were investigated in this paper. We brought a novel approach by building strong physical interactions for aniline oligomer self-assembly to enrich the design and enable the development of highly stretchable and conductive materials.

Results and discussion

1. Synthesis of the super stretchable electroactive elastomers

A series of super stretchable electroactive polyurethane-urea elastomers with different compositions were synthesized as shown in Scheme 1. To control the modulus of the materials, these elastomers were based on low molecular weight PLLA (M_n=1500) and poly(polyethylene glycol) (PEG, a widely used water soluble polymer) with different molecular weights (M_n=1000, 2050, 4000, or 6000). The molar ratio of PLLA and PEG was set at 1:1 to investigate the influence of the PEG segment's length on the elastomer's modulus. Meanwhile, an electroactive oligoaniline, amine-capped aniline trimer (AT) was added to endow this material with electroactivity. Elastomers with three different AT contents (wt%=3, 6, 12%) were synthesized to investigate the role of π-π stacking in micro-phase separation and mechanical properties. Dimethylol propionic acid (DMPA) has two hydroxyl end groups and a pendent carboxyl group, which could improve the hydrophilicity of polymer chain and generate ionic cross-linking by intermolecular doping with the AT segment. With a high reactivity towards activated hydrogen, hexamethylene diisocyanate (HDI) was used to connect all the segments covalently through a two-step polymerization scheme. A polyurethane-urea prepolymer capped by isocyanate groups was obtained in the first step. The prepolymer was then either cross-linked with trimethylolpropane (TMP) or terminated with n-propanol (P) to produce elastomers with either a cross-linked network or linear structure (Scheme 1). The resulting copolymers were coded via a nomenclature that indicates the length of the PEG chain, the concentration of AT, and the identity of the crosslinker (Table 1). For example, the copolymer PEG1k-AT6-TMP was synthesized from PEG1000 and PLLA1500, the content of AT in the prepolymer was 6%, and the prepolymer was cross-linked using TMP. Every copolymer contains 5% DMPA, except those marked with an 'nD,' which contain no DMPA. The copolymer's structure was confirmed by ^{1}HNMR (Figure 1), FT-IR (Figure S1), and GPC (Table S1).

Figure 1 shows a representative ^{1}H NMR spectrum of prepolymer PEG2k-AT6: ^{1}H NMR (400MHz, DMSO-d_6, δ): 7.40 (s, 2H, NH), 6.79 (d, 2H, Ar H), 6.76 (s, 2H, Ar H), 6.74 (s, 2H, Ar H) for AT segments, 5.21 (t, 2H, poly CH_2), 4.33 (t, 2H, CH_2 of EG), 1.48 (d, 6H, poly CH_3), 1.38 (d, 6H, end CH_3) for PLLA1500 segments, 3.42 (s, 4H, poly CH_2) for PEG segments, 7.16 (d, 2H, NH), 2.94 (t, 4H, CH_2), 1.09 (t, 8H, CH_2) for HDI segments, 4.03 (s, 4H, CH_2), 1.22 (s, 3H, CH_3) for DMPA segments. The existence of amide group (δ =7.16 ppm), along with the appearance of all characteristic hydrogen of segments in the spectrum, proved a successful polymerization.

Figure S1 shows the FT-IR spectra of PEG2k, AT, PLLA1500, and copolymer PEG2k-AT6-TMP. The characteristic absorption at 2260 cm^{-1} (N=C stretching) of NCO group was not observed in the copolymer spectrum, indicating a complete consumption of the isocyanate

group. A new peak at 1539 cm^{-1} is the absorption of the secondary amide band II, confirming the successful formation of amide groups from reactive hydrogen and isocyanate groups. The absorption band at 1503 cm^{-1} was assigned to the stretching of the benzenoid ring, indicating that AT segments were incorporated into copolymer chains. The PEG2k-AT6-TMP spectrum contains most of the characteristic component group absorptions, indicating successful copolymer synthesis. Furthermore, GPC measurements demonstrate that the copolymer molecular weight was much higher than the employed macromere, with a polydispersity between 1.4 and 1.8 (Table S1 in SI). Combined, the FT-IR, NMR and GPC measurements confirm successful synthesis of both the prepolymers and cross-linked copolymers.

2. Electroactivity of the copolymers

The copolymer electroactivity was studied using UV-visible spectroscopy. The absorption curves of AT, prepolymer PEG2k-AT6 and their camphorsulfonic acid (CSA)-doped samples in DMSO are shown in Figure 2A. For the AT sample (curve a), two absorption peaks were observed at 345 nm (π-π* benzenoid ring transition) and 589 nm (excitonic transition from benzenoid to quinoid ring). After the copolymerization, the π-π* transition absorption shifted to lower wave lengths (312 nm), as either PLLA or PEG segments decreased the conjugation length of AT. The excitonic transition of AT in the copolymer solution shifted to 561 nm, triggered by the formation of urea groups which decreased the electron density of the quinoid rings.[36] AT segment doping occurs via an oxidation reaction and results in transforming the benzenoid and quinoid rings to a structure with delocalized electrons and nitrogen ions.

After doping, a new peak appeared in the AT curve (curve b) at 404 nm – this was assigned to the absorption peak of the now-delocalized polaron. This phenomenon was also observed in the copolymer samples, with a new peak appearing at 414 nm after doping with CSA. Compared to the undoped prepolymer (curve c), the absorption at 312 nm shifted to 300 nm for the doped sample (curve d), and a wide peak at 910 nm appeared due to the delocalization of polaron along the polymer chain.[37]

The cyclic voltammogram of prepolymer PEG2k-AT6 is shown in Figure 2B. With increasing voltage, AT segments in the copolymer film underwent two oxidation transitions. The first oxidation of AT happened at 0.46 V, when the leucoemeraldine state transformed into an emeraldine state. Emeraldine AT was further oxidized to a pernigraniline state at 0.65 V. The two pairs of redox peaks indicated a copolymer with good electroactivity.

3. Mechanical properties and the mechanism for super stretchability

The mechanical properties of cross-linked networks and their corresponding linear copolymers are shown in Table 2. Some of the representative stress-strain curves of copolymers are displayed in Figure 3A–D. All the copolymers containing PEG4k and PEG6k segments do not have a rubber-like stress-strain curve. Copolymers based on low molecular weight PEG exhibit a modulus comparable to rat fresh nerve tissue and human cerebral blood vessels.[11–12] Among these materials, elastomer PEG2k-AT6-TMP possessed

the best mechanical properties, showing both high strength and excellent elasticity with a strain at break of 1643%.

Previous studies have demonstrated how substrate moduli effectively manipulate cell behavior in a manner similar to native soft tissues.[38–39] This elastomer possesses not only a proper modulus, but also stretchability comparable to highly stretchable hydrogels but with a much higher strength.[40–47] In addition, when compared to PLGA and PCL foam scaffolds used in bladder tissue engineering, our copolymers possess a 1 h to obtain a uniform dispersion liquid. The[48] A synergistic combination of physical interactions including π-π stacking between AT segments, hydrogen bonding and crystallization of the soft segments, and inter/intramolecular ionic interaction and chemical cross-linking may have resulted in the copolymer's high stretchability. The following studies were carried out to systematically examine each of them.

3.1 Microphase separation driven by self-assembly of aniline trimer—AT is a diamine hard segment with rigid benzenoid and quinoid rings which stacks easily in a poor solvent to form aggregates. AT rich domains exist in PEG2k-AT6-P and the hard domains from AT self-assembly likely play an important role in the copolymer super stretchability. To study the contribution of AT segments to the copolymer mechanical properties, we used hexanediamine (HDA) to take the place of the AT segments in PEG2k-AT6-P. HDA is a soft aliphatic diamine with a similar chemical structure and physical shape to AT diamine; however, it does not have the π-π stacking effect. Therefore the physical interactions among HDA should be substantially weaker than those among AT segments. As hypothesized, the formation of hard domains was impeded in PEG2k-HDA-P films. There is no obvious phase separation in the PEG2k-HDA-P film TEM micrograph (Figure 4A). The strength and strain at break of PEG2k-HDA-P decreased significantly to 1.9±0.2 MP and 448±34% (Table 2 and Figure 3A), indicating that AT is an irreplaceable hard segment for high stretchability. AT can completely dissolve in dimethyl formamide (DMF), which severely inhibits π-π stacking. After film fabrication in DMF solution, there is no obvious phase separation in the PEG2k-AT6-P thin film TEM micrograph (Figure 4C). PEG2k-AT6-P films fabricated from DMF solution also show a significantly decreased strain of 47% (Table 2 and Figure 3A), which was 33.5 times lower than that of the strain of films fabricated in tetrahydrofuran (THF). The strength and strain at break of PEG2k-AT6-P fabricated in THF were 11.0±0.6 MP and 1573±63%, respectively. These measurements were similar to PEG2k-AT6-TMP fabricated in THF, indicating that the mechanical properties were dominated by physical interactions rather than chemical cross-linking. Therefore, we concluded that the micro-phase separation of AT aggregates plays a predominant role for the super stretchability of these copolymer elastomers. Our data strongly suggests the critical role these aggregates play is due to AT segments forming hard domains in the elastomer films via self-assembly and subsequently serving as physical cross-links, which greatly increases the strength and stain at break of the materials.

Self-assembly of the phenyl ring structure is a well-known tool for fabricating various composite material structures. It is usually driven by molecule recognition, including π-π stacking.[49–51] π-π stacking is an important aspect for many material properties, including charge transport in organic electronics.[52] With the π-conjugated structure in an aniline

trimer segments, π-π stacking interactions can be easily established in a poor solvent.[53–54] Since the solubility of AT is poor in THF and good in DMSO, the sample PEG2k-AT6-P is dissolved in both solvents and UV-vis spectroscopy is utilized to study the π-π stacking of AT. The absorptions of π-π* and πB-πQ appear at 317 and 564 nm in DMSO and shift to 307 and 538 nm in THF due to the formation of π-π stacking of AT aggregates (Figure S2 in SI). The self-assembly of AT is further investigated by ^{1}H NMR spectra. PEG2k-AT6-P is dissolved in THF-d_8 and DMSO-d_6. To compare the concentrations of dissolved AT, the integral of a hydrogen from a methine group of the repeating unit of the PLLA segment was set as a constant. The integral of hydrogen from AT in DMSO is greater than that in THF (Figure S3 in SI). This demonstrates that the AT segment was partially encapsulated into self-assembled aggregates in THF, which cannot be detected by NMR.[55]

Meanwhile, the result of a dynamic light scattering (DLS) test of the sample PEG2k-AT6-P in THF indicates that the AT aggregates are present in the solution, and the size of the self-assembled aggregates is ~ 200 nm (Figure S4 in SI). These aggregates are also supposed to be produced during the elastomer film fabrication. As the solvent evaporates, AT segments precipitate around their aggregates to form hard domains (Figure 4B, D and E). These domains were separated by a soft polymer matrix, leading to the occurrence of micro-phase separation. The morphology of micro-phase separation in thin films of PEG2k-HDA-P and PEG2k-AT6-P can be observed via TEM (Figure 4A and B). There is no obvious phase separation in the PEG2k-HDA-P film as no rigid segment self-assembly occurs. The hard domains initiated from AT segment self-assembly are universally dispersed spheres with sizes ranging from 200 to 500 nm, as shown in Figure 4D. In copolymers containing aniline oligomer segments, phase separation triggered by self-assembly of aniline oligomer is also influenced by the soft segments[56]. Therefore, when aggregates were initiated in a THF suspension by AT segment self-assembly, soft chains such as PLA and PEG attached to AT were also involved in this procedure. The size of the hard domains is larger than AT aggregates in THF (200 nm) determined by DLS as more AT-rich polymer chains precipitate and assemble into aggregates with the evaporation of the solvent. Furthermore, this result is consistent with other reported aniline oligomer-based copolymer self-assembly sizes[57–59].

Because the hard domains are initiated from the self-assembly of AT, the domains' formation and morphology in the matrix of PU copolymer are directly related to the hard segment concentration. We synthesized samples with different AT concentrations (3%, 6% and 12%) to study the influence of hard segment concentration on mechanical properties and domain morphology. The modulus and stresses at the same strain values of the materials increased with increasing AT concentration (Figure S5 in SI). However the TEM micrographs showed that exorbitant amounts of AT formed irregular hard domains and jeopardized the uniformity of hard segment domain distribution. The size of the aggregates in PEG2k-AT12-P was more uneven than other copolymers with lower AT content (Figure S6 in SI). On the other hand, lowering the hard segment content of PEG2k-AT3-P weakened physical cross-linking. Hence intermediate AT concentrations generated proper levels of phase-separation and domain size and exhibited superior mechanical properties.

3.2 Crystallinity and chemical cross-linking—Crystallization is likely an important factor in a polymer's mechanical behavior.[60–61] The crystals in a polymer matrix serve as physical cross-links in a semi-crystalline material, and contribute to a higher modulus due to the highly oriented dense polymer chains. DSC measurements indicated that samples containing PEG4k and PEG6k segments have endothermic peaks at 45–55 °C, which resulted from PEG crystals melting (Figure S7 and Table S2). Due to the existence of PEG crystals as primary physical cross-links, all the samples containing PEG4k and PEG6k have significantly higher moduli than the PEG1k and PEG2k samples (Table 2, Figure 3B, and Table S3), and they increased correspondingly with increasing PEG content in the copolymers. The strain at break of the materials decreased accordingly.

The moduli of these elastomers are also influenced by chemical cross-links, but in a minor way. For the semi-crystalline samples (PEG4k-AT-TMP/P and PEG6k-AT-TMP/P), the values of melting point and crystallinity suggest that chemical cross-linking hinders the polymer chains' mobility, impeding the crystallization of the polymer (Figure 5). That is why linear copolymers PEG4k-AT6-P and PEG6k-AT6-P have higher moduli than their corresponding cross-linked copolymers (Table S3). DSC thermograms show that PEG crystals do not exist in either chemical cross-linked samples or linear samples of PEG1k and PEG2k; therefore, the Young's modulus of these amorphous elastomers increases after chemical cross-linking. In the meantime, the moduli of the PEG1k samples are slightly higher than PEG2k samples due to PEG1k-AT6-TMP's higher chemical cross-linking density (Table 2, Table S3 and Figure 3B).

3.3 Self-doping of AT—Electrostatic attraction is an important interaction in macromolecules.[62] Ionically cross-linked networks also play a role in the mechanical properties of supramolecules and hydrogels.[53, 63] The self-doping in polyaniline, generated by a negative charged group, is also an example of inter/intramolecular ionic cross-linking. The copolymers contain an acid group from DMPA and aniline oligomer AT between which doping reactions can occur (Figure 6). This phenomenon was demonstrated via XPS, confirming the existence of C-N^+ at a binding energy of 287.1 eV in the C1s spectrum (Figure 7) and N^+ at 401.2 eV in the N1s spectrum (Table S4 in SI) for a DMPA-containing PEG2k-AT6-TMP copolymer.[36] This indicates that there is ionic interaction between –COOH and AT segments in the elastomer PEG2k-AT6-TMP, while there is no such interaction in the control sample without DMPA, PEG2k-AT6-nD-TMP (Table S4 in SI). This strong inter/intra-molecular ionic interaction greatly enhances the strength of elastomers (Table 2). While some electrostatic interactions may break during deformation, new interactions may also form during the deformation, giving the elastomer an excellent strain at break (Figure 3C).

3.4 H-bonding interaction in the copolymers—Hydrogen bonding is a non-covalent linkage that can construct or enhance interactions between polymer chains.[64–65] The strong interactions between urethane and urea groups contribute to the physical cross-links, providing unique mechanical properties for PU polymers. Trifan et al. emphasized an ideal zig-zag chain structure for H-bonding formation in polyurethane.[61] The density of H-bonding in the networks was also influenced by the PEG length due to its high oxygen

content (Figure S8). To study how PEG segment length uniformity influenced mechanical properties, we synthesized the copolymer PEG1k+4k-AT6-TMP by using a mixture of PEG1000 and PEG4000 (molar ratio=2:1). Therefore, PEG1k+4k-AT6-TMP has the same PEG average molar molecular weight as sample PEG2k-AT6-TMP. However, compared to PEG2k-AT6-TMP, the PEG1k+4k-AT6-TMP sample has a more irregular structure which will hinder the matching of urethane(-urea) groups and decrease the density of H-bonding, reducing the physical cross-linking interactions during stretching (Figure 8). As expected, the measured strength and modulus of PEG1k+4k-AT6-TMP was notably lower than that of PEG2k-AT6-TMP (Table 2 and Figure 3D). However, its strain at break remained very large, suggesting that H-bonding was not a major contributor to the super stretchability.

4. Conductivity and biocompatibility of super stretchable materials

The electrical conductivity of the PEG2k-AT6-P was on the order of 10^{-6} S/cm. To improve the conductivity of the super stretchable materials, the copolymer was blended with conductive polyaniline nanofibers (PANI) or nano-sized carbon black (CB). The resulting conductivity and mechanical properties of these composite materials are listed in Table 3. When the filler content was fixed at 2% (w/w), the conductivity of copolymer/PANI nanofiber composite was three times that of the copolymer/carbon black composite. To understand this difference between the two fillers, the morphologies of the copolymer, PANI nanofibers, copolymer/PANI nanofiber composite, copolymer/carbon black composite were examined under TEM (Figure S9). It appears that the PANI nanofibers likely more efficiently connect the hard domains than the carbon black powder in improving the conductivity[66]. However, the spherical shape allows a higher percentage of carbon black to be easily incorporated into the composite to further improve the conductivity (Table 3). While the modulus was slightly increased by the fillers, the conductivity was increased by a few orders of magnitude. Excitingly, the super stretchability of the composite materials was largely maintained, demonstrating the high potential of the novel copolymer for soft tissue regeneration applications.

In addition, the biocompatibility of films PEG2k-AT3-P, PEG2k-AT6-P and PEG2k-AT12-P was evaluated using C2C12 cells (a murine myoblast cell line). Compared to a PLLA control group, no cytotoxicity was observed with any of the samples (Figure S10 in SI). Thus, our copolymers could potentially find applications in soft tissue engineering.

Conclusions

A series of super stretchable electroactive polyurethane-urea elastomers based on polylactide and aniline trimer were successfully synthesized and characterized. The copolymers showed an excellent strain at break of more than 1600% and possessed a modulus similar to soft tissues. The mechanism of the super stretchability was thoroughly investigated. The micro-phase separation driven by the self-assembly of aniline trimer due primarily to π-π stacking in THF resulted in strong physically associated cross-linked hard domain formation. The distribution of the hard domains in a uniform soft matrix plays a decisive role for the super strain at break. The roles of crystallinity, chemical cross-linking, hydrogen bonding and ionic cross-linking contributed only in a minor way to the materials'

super strain at break. Furthermore, the conductivity of the copolymer elastomers was increased by several orders of magnitude by blending polyaniline nanofibers or nanosized carbon black, while maintaining a high strain at break. Because of the biocompatibility of these copolymers, the new elastomers have high potentials to be used for biomedical applications, including the regeneration of nerve, blood vessels, cardiac muscle and other soft tissues to be explored in the future.

Experimental section

1. Synthesis of PLLA1500 and AT

L-lactide, initiator ethylene glycol and the catalyst stannous octoate were added into a single-necked flask under the protection of nitrogen. The polymerization was carried out at 110 °C for 48 h to obtain a white waxy product. The product was purified by dissolution in chloroform and precipitation into cold ether three times to remove residual monomer and catalyst. The powder was vacuum dried for 2 days before use. Characterization: ^{1}H NMR (400MHz, $CDCl_3$) δ 5.18 (t, 2H, poly –CH–), 4.38 (t, 4H, –CH_2– of EG), 4.37 (t, 2H, end –CH–), 1.60 (d, 6H, poly –CH_3), 1.51 (d, 6H, end –CH_3). IR (neat, cm^{-1}) 3690 (m, ν_{OH}), 2996 (w, ν_{as} CH_3), 2959 (w, ν_{OH}), 1754 (s, $\nu_{C=O}$), 1455 (s, δ_s CH_3), 1383 (w, δ_{as} CH_3), 1370, 1359 (w, δ_s C-CH_3), 1181, 1085 (m, ν_{O-C-O}), 871, 755 (s, γ C-CH_3). AT was synthesized through an oxidative coupling reaction reported by Wei et al.[62] ^{1}H NMR (400MHz, DMSO-d_6) δ 5.45 (s, 4H, -NH_2), 6.95 (s, 4H, Ar-H), 6.79 (d, 4H, Ar-H), 6.62 (d, 4H, Ar-H). IR (neat, cm^{-1}) 3310 (m, ν_{NH}), 3206 (m, ν_{NH}), 1598 (s, $\nu_{C=C}$ of quinoid ring), 1504 (s, $\nu_{C=C}$ of benzenoid rings).

2. Synthesis of prepolymers

Before the reaction, PEG (0.50 mmol), PLLA (0.50 mmol), DMPA (0.74 mmol) and AT (predetermined amount in Table 1) were mixed and dehydrated in a two-necked flask at 110 °C for 2 h. The system was then cooled to 70 °C, and the mixture was dissolved in THF and NMP (Vol:Vol = 5:1) under nitrogen protection. HDI (n_{NCO}/n_H = 1.05) and catalyst $Sn(Oct)_2$ (molar ratio to macromere = 1:500) were then added to the solution. The prepolymerization was carried out for 4 h at 70 °C. After cooling, the prepolymer were purified with repeated dissolution in THF and precipitation into cold ether three times.

3. Synthesis of copolymers and film casting

For the cross-linked or linear samples, TMP or n-propanol respectively were added to prepolymer solution in THF. The solution was then cast into a Teflon Petri dish. The dish was sealed by tinfoil to slow down the solvent evaporation rate and placed in an oven at 70 °C. After 4 h of cross-linking reaction, the film was vacuum dried for 24 h to remove residual solvents. Thicknesses were around 500 μm according to a thickness meter (Mitutoyo Absolute).

4. Synthesis of polyaniline nanofibers

Polyaniline nanofibers were synthesized through a interfacial polymerization reported previously.[67] In summary, 3.2 mmol of aniline was dissolved in 10 mL of dichloromethane and 0.8 mmol of ammonium peroxydisulfate was dissolved in 10 mL of 1 M HCl solution.

Both the oil and water phase were transferred into a 20 mL vial and the polymerization was carried out overnight at room temperature. The product was filtrated and washed twice with deionized water to obtain doped polyaniline nanofibers. The product was vacuum dried for 2 days before use.

5. Fabrication and conductivity measurement of blend films

A predetermined amount of conductive fillers were added to a 20% (wt/vol) copolymer solution in THF. The mixture was stirred for 1 h to obtain a uniform dispersion liquid. The mixture was cast into a Petri dish and dried in a 50 °C oven. The films were subsequently vacuum dried and removed from the Petri dishes. The electrical resistance R of the blended films was determined with an HP 4284A bridge, and the conductivity σ was calculated based on the following formula: $\sigma = l / RS$, where l and S are the length and sectional area of materials, respectively.

6. Cytotoxicity test

A series of PLLA, PEG2k-AT3-P, PEG2k-AT6-P and PEG2k-AT12-P extracts with concentrations of 1.5625, 3.125, 6.25, 12.5, and 25 mg/mL respectively were prepared by soaking each polymer with cell culture medium for 48 h at 37 °C. The polymers were next sterilized by ethylene oxide treatment. Rat C2C12 cells were incubated at 37 °C in a humidified incubator containing 5% CO_2. The complete growth medium consisted of DMEM, 10% fetal bovine serum, 1.0×10^5 U/L penicillin and 100 mg/L streptomycin. 2000 C2C12 cells suspended in 100 μL of the complete growth medium were seeded in each well of a 96-well plate. After being cultured for 24 h, the medium was changed with 100 μL of the medium containing the polymer extract. After 4 days of cell culture with a daily change of media + polymer extract, 10 μL alamaBlue® (Invitrogen) reagent was added to each well. The cells were cultured for 6 hours in the incubator protected from light, then 100 μl of the medium from each well was pipetted into a 96-well black plate. Fluorescence was measured by a microplate reader (Molecular Devices) with excitation and emission wavelengthes of 560 nm and 594 nm, respectively. Each group contained 6 repeated tests in total.

Supplementary Material

Refer to Web version on PubMed Central for supplementary material.

Acknowledgments

The authors gratefully acknowledge the National Natural Science Foundation of China (grant number 21304073), the National Institutes of Health of the US (NHLBI HL11403) and Xi'an Jiaotong University for financial support of this work.

References

1. Serrano MC, Chung EJ, Ameer GA. Advances and Applications of Biodegradable Elastomers in Regenerative Medicine. Adv Funct Mater. 2010; 20:192–208.
2. Liu QY, Jiang L, Shi R, Zhang LQ. Synthesis, preparation, in vitro degradation, and application of novel degradable bioelastomers-A review. Prog Polym Sci. 2012; 37:715–765.

3. Hung KC, Tseng CS, Hsu S-h. Synthesis and 3D Printing of Biodegradable Polyurethane Elastomer by a Water-Based Process for Cartilage Tissue Engineering Applications. Adv Healthc Mater. 2014; 3:1578–1587. [PubMed: 24729580]
4. Sasaki M, Karikkineth BC, Nagamine K, Kaji H, Torimitsu K, Nishizawa M. Highly Conductive Stretchable and Biocompatible Electrode–Hydrogel Hybrids for Advanced Tissue Engineering. Adv Healthc Mater. 2014; 3:1919–1927. [PubMed: 24912988]
5. Wang YD, Ameer GA, Sheppard BJ, Langer R. A tough biodegradable elastomer. Nat Biotechnol. 2002; 20:602–606. [PubMed: 12042865]
6. Bruggeman JP, de Bruin BJ, Bettinger CJ, Langer R. Biodegradable poly(polyol sebacate) polymers. Biomaterials. 2008; 29:4726–4735. [PubMed: 18824260]
7. Yang J, Webb AR, Ameer GA. Novel citric acid-based biodegradable elastomers for tissue engineering. Adv Mater. 2004; 16:511.
8. Helminen AO, Korhonen H, Seppala JV. Cross-linked poly(epsilon-caprolactone/D, L-lactide) copolymers with elastic properties. Macromol Chem Phys. 2002; 203:2630–2639.
9. Heijkants R, van Calck RV, van Tienen TG, de Groot JH, Buma P, Pennings AJ, Veth RPH, Schouten AJ. Uncatalyzed synthesis, thermal and mechanical properties of polyurethanes based on poly(epsilon-caprolactone) and 1,4-butane diisocyanate with uniform hard segment. Biomaterials. 2005; 26:4219–4228. [PubMed: 15683644]
10. Wang WS, Ping P, Yu HJ, Chen XS, Jing XB. Synthesis and characterization of a novel biodegradable, thermoplastic polyurethane elastomer. J Polym Sci Part A: Polym Chem. 2006; 44:5505–5512.
11. Borschel GH, Kia KF, Kuzon WM, Dennis RG. Mechanical properties of acellular peripheral nerve. J Surg Res. 2003; 114:133–139. [PubMed: 14559438]
12. Monson KL, Goldsmith W, Barbaro NM, Manley GT. Axial mechanical properties of fresh human cerebral blood vessels. J Biomech Eng Trans ASME. 2003; 125:288–294.
13. Nair DP, Podgorski M, Chatani S, Gong T, Xi WX, Fenoli CR, Bowman CN. The Thiol-Michael Addition Click Reaction: A Powerful and Widely Used Tool in Materials Chemistry. Chem Mater. 2014; 26:724–744.
14. Gilbert PM, Havenstrite KL, Magnusson KEG, Sacco A, Leonardi NA, Kraft P, Nguyen NK, Thrun S, Lutolf MP, Blau HM. Substrate Elasticity Regulates Skeletal Muscle Stem Cell Self-Renewal in Culture. Science. 2010; 329:1078–1081. [PubMed: 20647425]
15. Choi JS, Harley BAC. The combined influence of substrate elasticity and ligand density on the viability and biophysical properties of hematopoietic stem and progenitor cells. Biomaterials. 2012; 33:4460–4468. [PubMed: 22444641]
16. Nassif N, Gobeaux F, Seto J, Belamie E, Davidson P, Panine P, Mosser G, Fratzl P, Guille MMG. Self-Assembled Collagen-Apatite Matrix with Bone-like Hierarchy. Chem Mater. 2010; 22:3307–3309.
17. Zhao B, Hu H, Mandal SK, Haddon RC. A bone mimic based on the self-assembly of hydroxyapatite on chemically functionalized single-walled carbon nanotubes. Chem Mater. 2005; 17:3235–3241.
18. Zhang QM, Li HF, Poh M, Xia F, Cheng ZY, Xu HS, Huang C. An all-organic composite actuator material with a high dielectric constant. Nature. 2002; 419:284–287. [PubMed: 12239563]
19. Pelrine R, Kornbluh R, Pei QB, Joseph J. High-speed electrically actuated elastomers with strain greater than 100%. Science. 2000; 287:836–839. [PubMed: 10657293]
20. Mannsfeld SC, Tee BC, Stoltenberg RM, Chen CVH, Barman S, Muir BV, Sokolov AN, Reese C, Bao Z. Highly sensitive flexible pressure sensors with microstructured rubber dielectric layers. Nat Mater. 2010; 9:859–864. [PubMed: 20835231]
21. Zhai DY, Liu BR, Shi Y, Pan LJ, Wang YQ, Li WB, Zhang R, Yu GH. Highly Sensitive Glucose Sensor Based on Pt Nanoparticle/Polyaniline Hydrogel Heterostructures. Acs Nano. 2013; 7:3540–3546. [PubMed: 23472636]
22. Brochu P, Pei QB. Advances in Dielectric Elastomers for Actuators and Artificial Muscles. Macromol Rapid Commun. 2010; 31:10–36. [PubMed: 21590834]
23. Rajagopalan M, Oh IK. Fullerenol-Based Electroactive Artificial Muscles Utilizing Biocompatible Polyetherimide. Acs Nano. 2011; 5:2248–2256. [PubMed: 21332175]

24. Shi GX, Rouabhia M, Wang ZX, Dao LH, Zhang Z. A novel electrically conductive and biodegradable composite made of polypyrrole nanoparticles and polylactide. Biomaterials. 2004; 25:2477–2488. [PubMed: 14751732]
25. Wong JY, Langer R, Ingber DE. Electrically conducting polymers can noninvasively control the shape and growth of mammalian cells. PNAS. 1994; 91:3201–3204. [PubMed: 8159724]
26. Guo BL, Glavas L, Albertsson AC. Biodegradable and electrically conducting polymers for biomedical applications. Prog Polym Sci. 2013; 38:1263–1286.
27. Bhadra S, Khastgir D, Singha NK, Lee JH. Progress in preparation, processing and applications of polyaniline. Prog Polym Sci. 2009; 34:783–810.
28. Salvatierra RV, Cava CE, Roman LS, Zarbin AJG. ITO-Free and Flexible Organic Photovoltaic Device Based on High Transparent and Conductive Polyaniline/Carbon Nanotube Thin Films. Adv Funct Mater. 2013; 23:1490–1499.
29. Shao L, Jeon JW, Lutkenhaus JL. Polyaniline/Vanadium Pentoxide Layer-by-Layer Electrodes for Energy Storage. Chem Mater. 2012; 24:181–189.
30. Peng CW, Hsu C-h, Lin K-H, Li P-L, Hsieh M-F, Wei Y, Yeh J-M, Yu Y-H. Electrochemical corrosion protection studies of aniline-capped aniline trimer-based electroactive polyurethane coatings. Electrochim Acta. 2011; 58:614–620.
31. Guo BL, Finne-Wistrand A, Albertsson AC. Molecular architecture of electroactive and biodegradable copolymers composed of polylactide and carboxyl-capped aniline trimer. Biomacromolecules. 2010; 11:855–863. [PubMed: 20201489]
32. Guo BL, Finne-Wistrand A, Albertsson AC. Degradable and electroactive hydrogels with tunable electrical conductivity and swelling behavior. Chem Mater. 2011; 23:1254–1262.
33. Guo BL, Sun Y, Finne-Wistrand A, Mustafa K, Albertsson AC. Electroactive tubular porous scaffolds with degradability and non-cytotoxicity for neural tissue regeneration. Acta Biomater. 2012; 8:144–153. [PubMed: 21985870]
34. Wei ZX, Laitinen T, Smarsly B, Ikkala O, Faul CFJ. Self-assembly and electrical conductivity transitions in conjugated oligoaniline - Surfactant complexes. Angew Chem Int Ed Engl. 2005; 44:751–756. [PubMed: 15612075]
35. Wang Y, Tran HD, Liao L, Duan XF, Kaner RB. Nanoscale Morphology, Dimensional Control, and Electrical Properties of Oligoanilines. J Am Chem Soc. 2010; 132:10365–10373. [PubMed: 20662516]
36. Guo B, Finne-Wistrand A, Albertsson AC. Universal two-step approach to degradable and electroactive block copolymers and networks from combined ring-opening polymerization and post-functionalization via oxidative coupling reactions. Macromolecules. 2011; 44:5227–5236.
37. Gao J, Liu DG, Sansiñena JM, Wang HL. Synthesis and Characterization of Electrochromic Polyamides with Well-Defined Molecular Structures and Redox Properties. Adv Funct Mater. 2004; 14:537–543.
38. Ghosh K, Pan Z, Guan E, Ge S, Liu Y, Nakamura T, Ren XD, Rafailovich M, Clark RAF. Cell adaptation to a physiologically relevant ECM mimic with different viscoelastic properties. Biomaterials. 2007; 28:671–679. [PubMed: 17049594]
39. Engler AJ, Sen S, Sweeney HL, Discher DE. Matrix Elasticity Directs Stem Cell Lineage Specification. Cell. 2006; 126:677–689. [PubMed: 16923388]
40. Sun JY, Zhao XH, Illeperuma WRK, Chaudhuri O, Oh KH, Mooney DJ, Vlassak JJ, Suo ZG. Highly stretchable and tough hydrogels. Nature. 2012; 489:133–136. [PubMed: 22955625]
41. Yang CH, Wang MX, Haider H, Yang JH, Sun JY, Chen YM, Zhou JX, Suo ZG. Strengthening Alginate/Polyacrylamide Hydrogels Using Various Multivalent Cations. ACS Appl Mater Interfaces. 2013; 5:10418–10422. [PubMed: 24128011]
42. Ning JY, Li G, Haraguchi K. Synthesis of Highly Stretchable, Mechanically Tough, Zwitterionic Sulfobetaine Nanocomposite Gels with Controlled Thermosensitivities. Macromolecules. 2013; 46:5317–5328.
43. Chen BH, Lu JJ, Yang CH, Yang JH, Zhou JX, Chen YM, Suo ZG. Highly Stretchable and Transparent Ionogels as Nonvolatile Conductors for Dielectric Elastomer Transducers. ACS Appl Mater Interfaces. 2014; 6:7840–7845. [PubMed: 24758275]

44. Xia LW, Xie R, Ju XJ, Wang W, Chen QM, Chu LY. Nano-structured smart hydrogels with rapid response and high elasticity. Nat Commun. 2013; 4
45. Cui YL, Tan M, Zhu AD, Guo MY. Mechanically strong and stretchable PEG-based supramolecular hydrogel with water-responsive shape-memory property. J Mat Chem B. 2014; 2:2978–2982.
46. Tan M, Zhao TT, Huang H, Guo MY. Highly stretchable and resilient hydrogels from the copolymerization of acrylamide and a polymerizable macromolecular surfactant. Polym Chem. 2013; 4:5570–5576.
47. Wei Z, Yang JH, Zhou JX, Xu F, Zrinyi M, Dussault PH, Osada Y, Chen YM. Self-healing gels based on constitutional dynamic chemistry and their potential applications. Chem Soc Rev. 2014; 43:8114–8131. [PubMed: 25144925]
48. Baker SC, Rohman G, Southgate J, Cameron NR. The relationship between the mechanical properties and cell behaviour on PLGA and PCL scaffolds for bladder tissue engineering. Biomaterials. 2009; 30:1321–1328. [PubMed: 19091399]
49. Wang S, Goh BM, Manga KK, Bao QL, Yang P, Loh KP. Graphene as Atomic Template and Structural Scaffold in the Synthesis of Graphene-Organic Hybrid Wire with Photovoltaic Properties. Acs Nano. 2010; 4:6180–6186. [PubMed: 20825226]
50. Abraham GA, Marcos-Fernández A, Román JS. Bioresorbable poly (ester-ether urethane) s from L-lysine diisocyanate and triblock copolymers with different hydrophilic character. J Biomed Mater Res A. 2006; 76:729–736. [PubMed: 16317720]
51. Shi Y, van der Meel R, Theek B, Oude Blenke E, Pieters EH, Fens MH, Ehling J, Schiffelers RM, Storm G, van Nostrum CF, Lammers T, Hennink WE. Complete Regression of Xenograft Tumors upon Targeted Delivery of Paclitaxel via Pi-Pi Stacking Stabilized Polymeric Micelles. Acs Nano. 2015; 9:3740–52. [PubMed: 25831471]
52. Okamoto T, Nakahara K, Saeki A, Seki S, Oh JH, Akkerman HB, Bao ZN, Matsuo Y. Aryl-Perfluoroaryl Substituted Tetracene: Induction of Face-to-Face pi-pi Stacking and Enhancement of Charge Carrier Properties. Chem Mater. 2011; 23:1646–1649.
53. Sun JY, Zhao X, Illeperuma WR, Chaudhuri O, Oh KH, Mooney DJ, Vlassak JJ, Suo Z. Highly stretchable and tough hydrogels. Nature. 2012; 489:133–136. [PubMed: 22955625]
54. De Groot J, De Vrijer R, Wildeboer B, Spaans C, Pennings A. New biomedical polyurethane ureas with high tear strengths. Polym Bull. 1997; 38:211–218.
55. Guo B, Finne-Wistrand A, Albertsson AC. Simple Route to Size-Tunable Degradable and Electroactive Nanoparticles from the Self-Assembly of Conducting Coil-Rod-Coil Triblock Copolymers. Chem Mater. 2011; 23:4045–4055.
56. Huang LH, Hu J, Lang L, Wang X, Zhang PB, Jing XB, Wang XH, Chen XS, Lelkes PI, MacDiarmid AG, Wei Y. Synthesis and characterization of electroactive and biodegradable ABA block copolymer of polylactide and aniline pentamer. Biomaterials. 2007; 28:1741–1751. [PubMed: 17218007]
57. Wang HF, Han YC. Vesicles Formed by Oligostyrene-block-Oligoaniline-block-Oligostyrene Triblock Oligomer. Macromol Rapid Commun. 2009; 30:521–527. [PubMed: 21706635]
58. Xiong W, Wang HF, Han YC. Fibrils Formed by Dendron-b-oligoaniline-b-dendron Block Co-oligomer. Macromol Rapid Commun. 2010; 31:1886–1891. [PubMed: 21567608]
59. Lang L, Zhuang XL, Liu YD, Zhang PB, Chen XS, Wei Y. Synthesis, Characterization and Self-Assembly of PEG-Aniline Tetramer Block Copolymer. Chem J Chin Univ -Chin. 2011; 32:411–415.
60. Thompson S. An overview of nickel–titanium alloys used in dentistry. Int Endod J. 2000; 33:297–310. [PubMed: 11307203]
61. Lemstra PJ. Confined polymers crystallize. Science. 2009; 323:725–726. [PubMed: 19197049]
62. Wei Y, Yang C, Ding T. A one-step method to synthesize N, N′-bis (4′-aminophenyl)-1, 4-quinonenediimine and its derivatives. Tetrahedron Lett. 1996; 37:731–734.
63. Sun TL, Kurokawa T, Kuroda S, Ihsan AB, Akasaki T, Sato K, Haque MA, Nakajima T, Gong JP. Physical hydrogels composed of polyampholytes demonstrate high toughness and viscoelasticity. Nat Mater. 2013; 12:932–937. [PubMed: 23892784]

64. Saito T, Furuta T, Hwang JH, Kuramoto S, Nishino K, Suzuki N, Chen R, Yamada A, Ito K, Seno Y, Nonaka T, Ikehata H, Nagasako N, Iwamoto C, Ikuhara Y, Sakuma T. Multifunctional Alloys Obtained via a Dislocation-Free Plastic Deformation Mechanism. Science. 2003; 300:464–467. [PubMed: 12702870]

65. Kim BS, Park SW, Hammond PT. Hydrogen-bonding layer-by-layer assembled biodegradable polymeric micelles as drug delivery vehicles from surfaces. Acs Nano. 2008; 2:386–392. [PubMed: 19206641]

66. Lin YF, Chen CH, Xie WJ, Yang SH, Hsu CS, Lin MT, Jian WB. Nano Approach Investigation of the Conduction Mechanism in Polyaniline Nanofibers. Acs Nano. 2011; 5:1541–1548. [PubMed: 21280617]

67. Huang JX, Kaner RB. A general chemical route to polyaniline nanofibers. J Am Chem Soc. 2004; 126:851–855. [PubMed: 14733560]

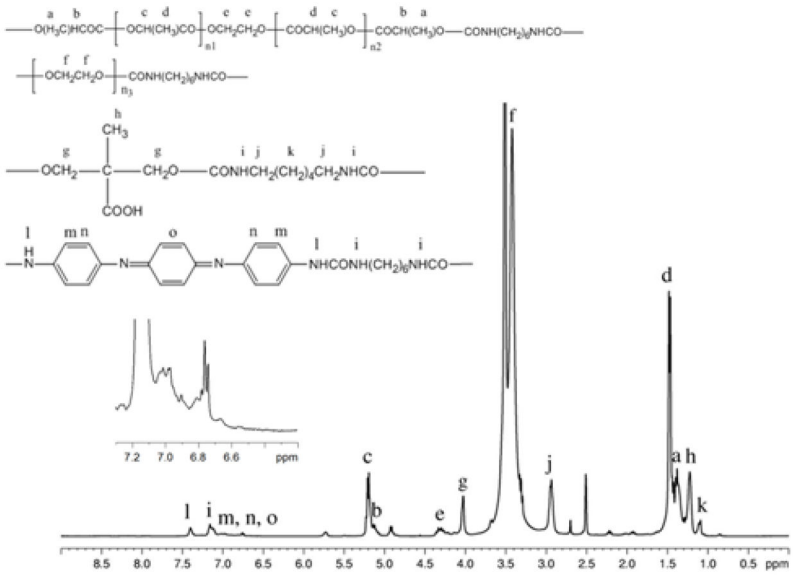

Figure 1.

^{1}H NMR spectrum of prepolymer PEG2k-AT6 in DMSO-d_6.

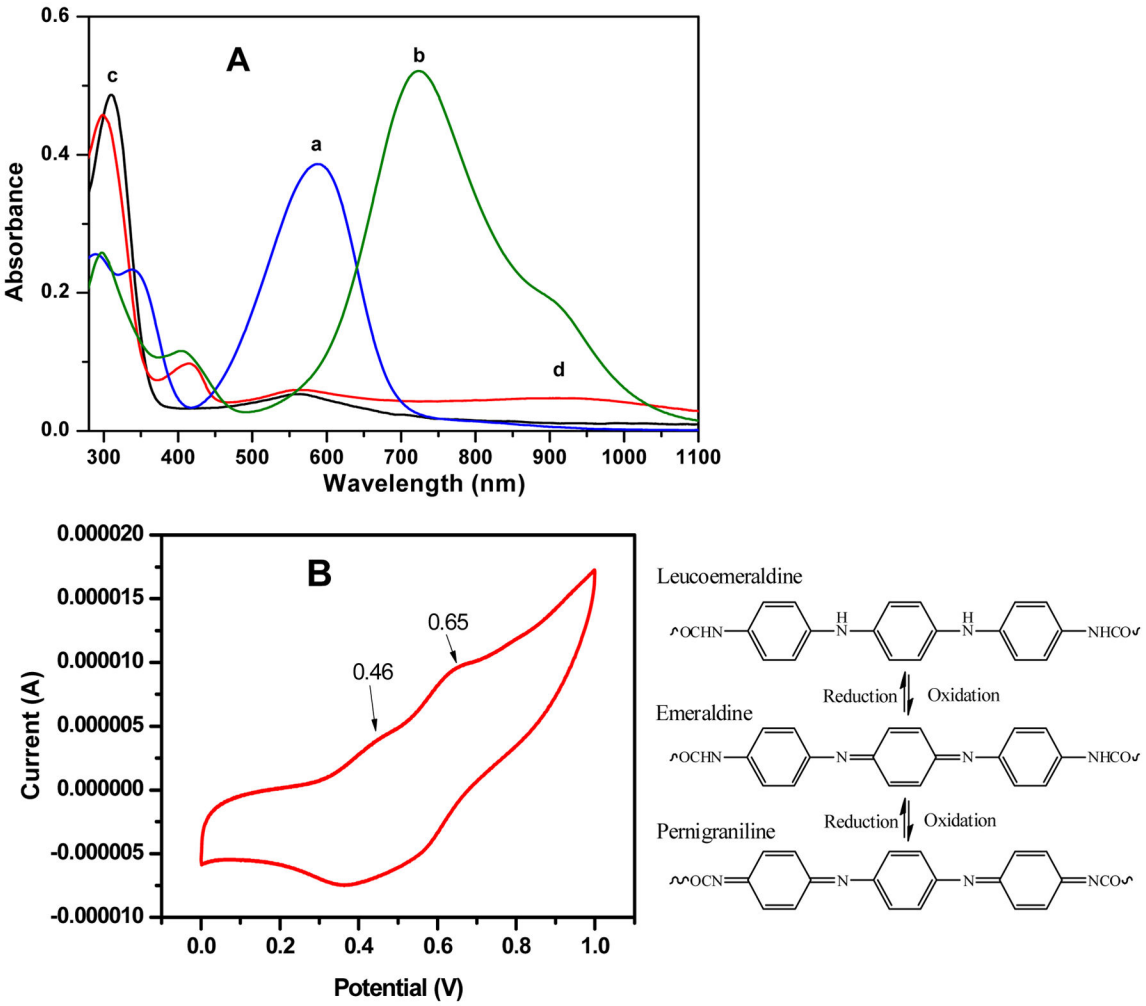

Figure 2.

(A): The UV-vis spectra of: (a) AT, (b) doped AT, (c) PEG2k-AT6 prepolymer, and (d) PEG2k-AT6 prepolymer doped with CSA. (B): Cyclic voltammogram of copolymer PEG2k-AT6-TMP film and molecular structure of copolymers at various oxidation states.

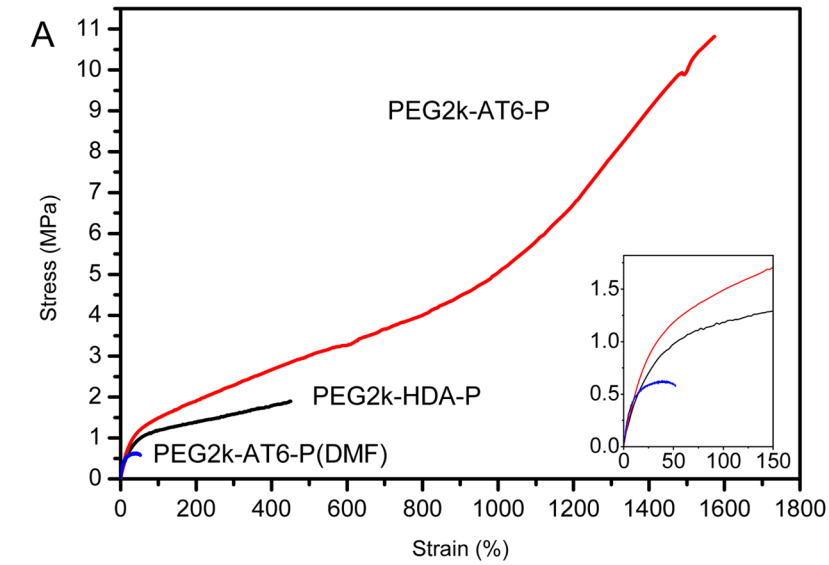

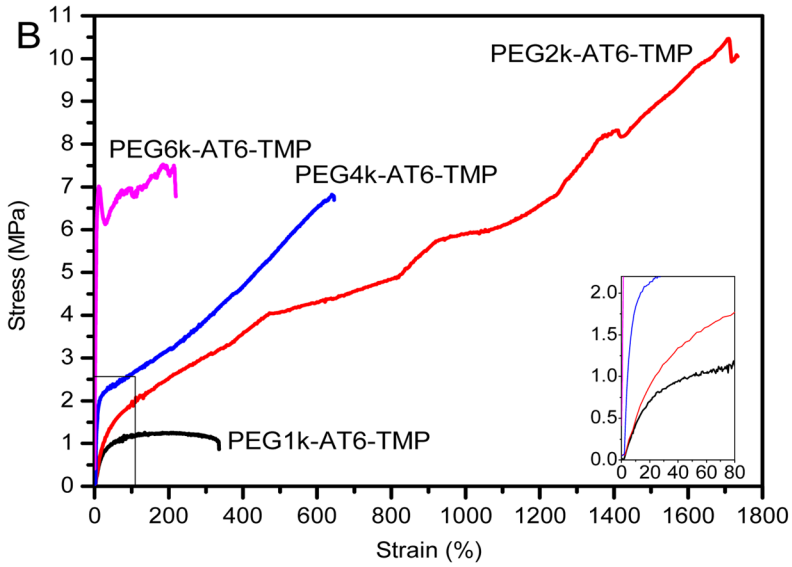

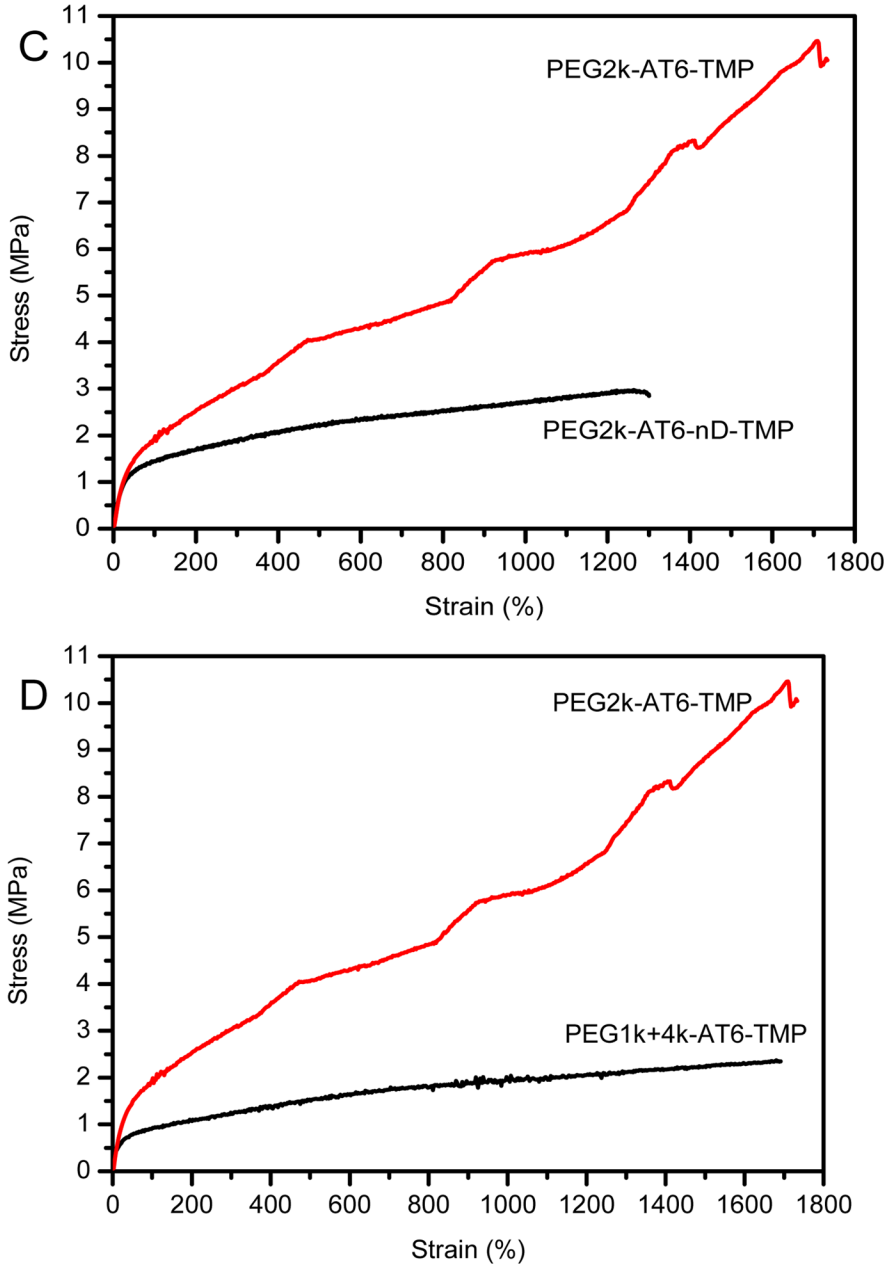

Figure 3.

Representative strain-stress curves of (A): PEG2k-AT6-P and PEG2k-HDA-P; (B): PEG6k-AT6-TMP, PEG4k-AT6-TMP, PEG2k-AT6-TMP and PEG1k-AT6-TMP; (C): PEG2k-AT6-TMP and PEG2k-AT6-nD-TMP; and (D): PEG2k-AT6-TMP and PEG1k+4k-AT6-TMP films.

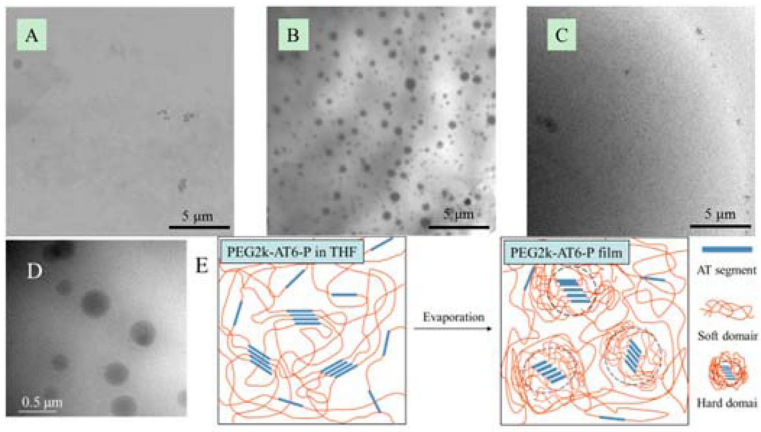

Figure 4.

TEM pictures of copolymer thin films and schematic model of hard domain formation in PEG2k-AT6-P film. (A): PEG2k-HDA-P thin films fabricated from THF solution; (B): PEG2k-AT6-P thin films fabricated from THF solution; (C): PEG2k-AT6-P thin films fabricated from DMF solution; (D): magnified picture of PEG2k-AT6-P thin film from THF showing the hard domains; and (E): the model of hard segment domains in PEG2k-AT6-P film.

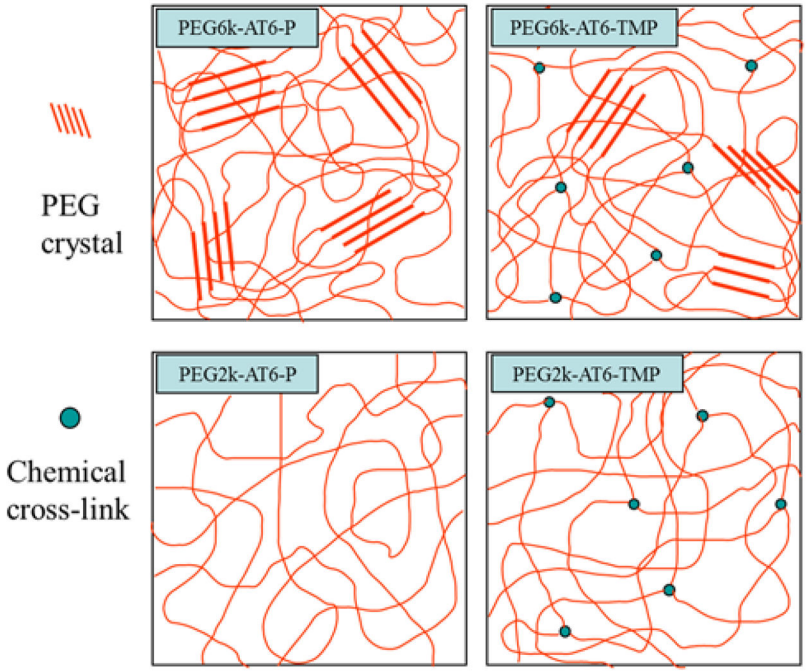

Figure 5.
Schematic model of PEG crystal and chemical cross-links interactions in copolymers.

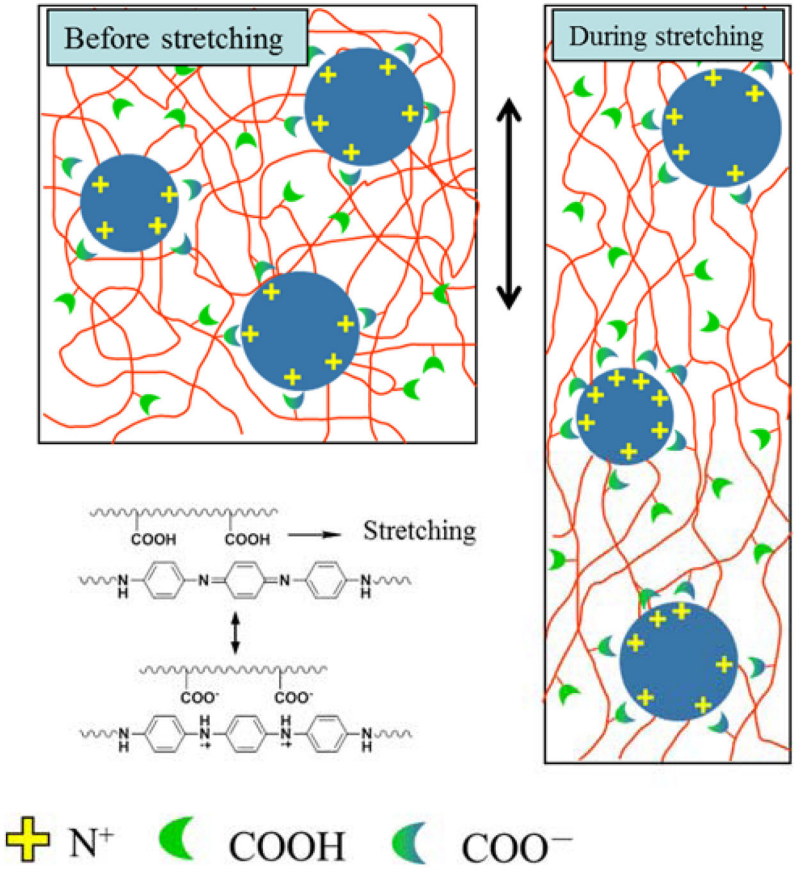

Figure 6.
Schematic model of ionic interactions via self-doping in copolymers.

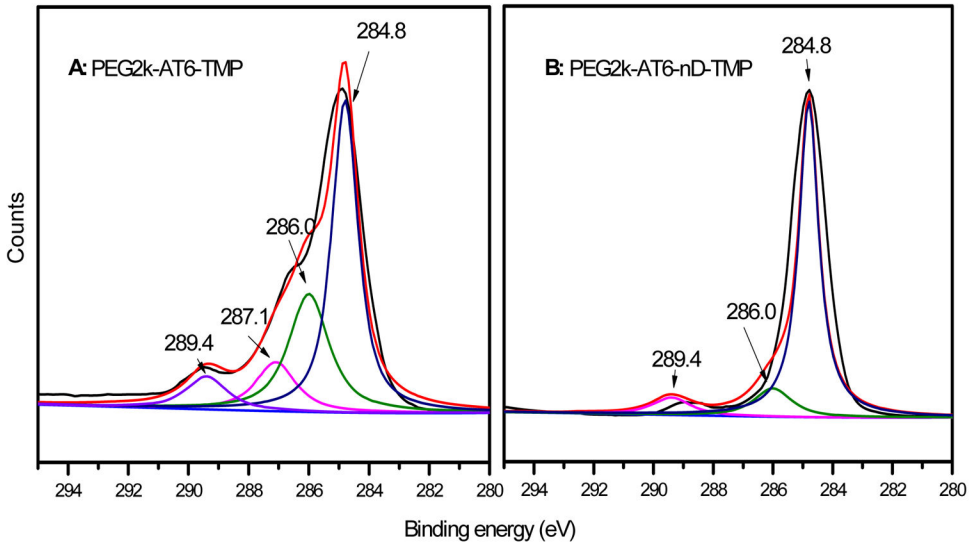

Figure 7.
XPS C1s spectra of the copolymers: (A) PEG2k-AT6-TMP, and (B) PEG2k-AT6-nD-TMP.

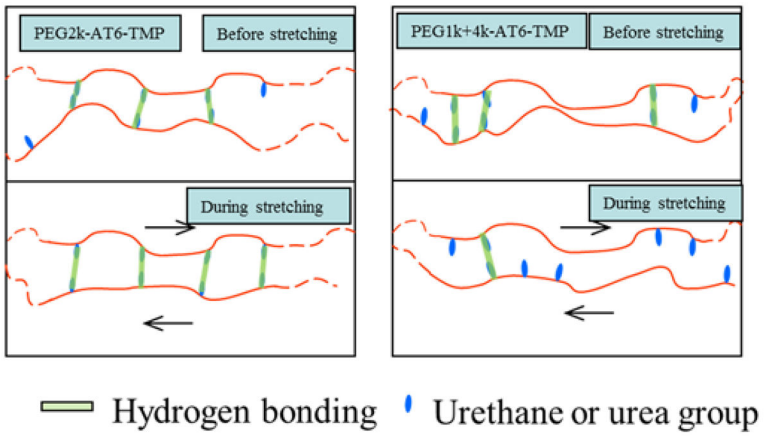

Figure 8.
Schematic model of hydrogen bonding matching in copolymers with even and uneven PEG segment lengths.

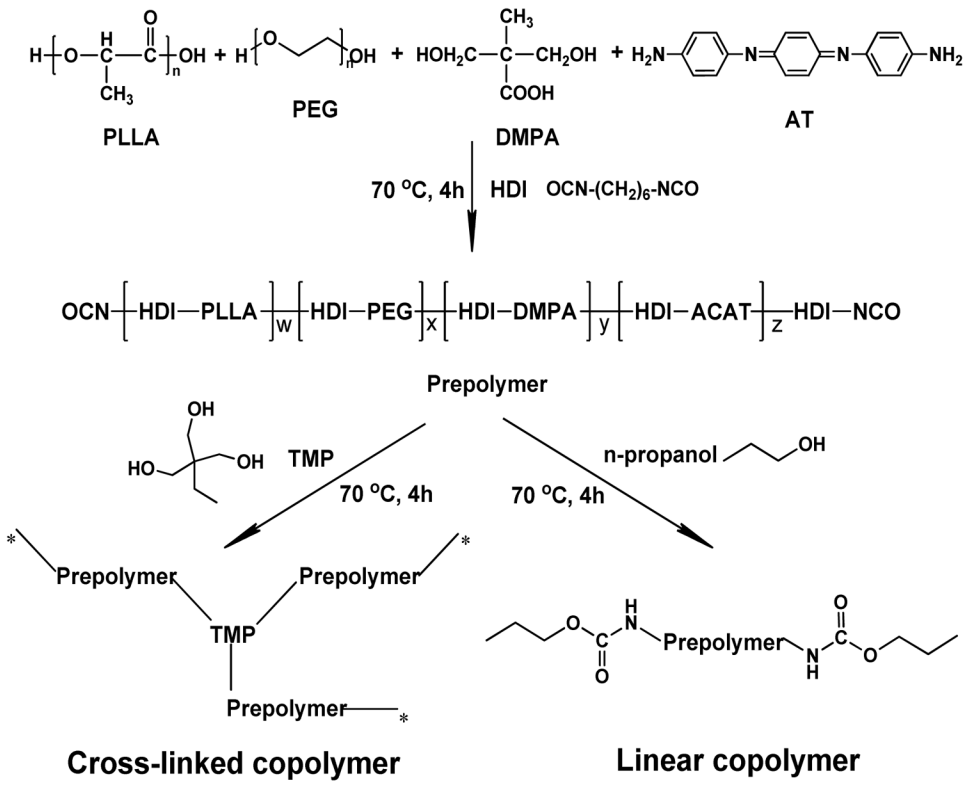

Scheme 1.
Synthetic scheme of the electroactive network and linear copolymers.

Table 1

Nomenclature of elastomer samples

Sample code	M_n of PLLA	Wt% of AT in prepolymer	Wt% of DMPA in prepolymer	M_n of PEG
PEG1k-AT6-TMP(P)	1500	6	5	1000
PEG2k-AT6-TMP(P)	1500	6	5	2050
PEG4k-AT6-TMP(P)	1500	6	5	4000
PEG6k-AT6-TMP(P)	1500	6	5	6000
PEG2k-AT3-P	1500	3	5	2050
PEG2k-AT12-P	1500	12	5	2050
PEG2k-AT6-nD-TMP	1500	6	0	2050
PEG1k+4k-AT6-TMP	1500	6	5	1k,4k

Table 2

Mechanical properties of copolymers and networks

Samples	Strength (MPa)	Strain (%)	Young's Modulus (MPa)
PEG1k-AT6-TMP	1.3±0.1	333±5	6.0±0.8
PEG2k-AT6-TMP	10.1±0.8	1643±157	4.2±1.2
PEG4k-AT6-TMP	6.5±0.5	597±68	29.2±1.6
PEG6k-AT6-TMP	8.2±1.1	242±4	189.9±8.2
PEG2k-AT3-TMP	6.7±0.2	983±52	4.4±0.4
PEG2k-AT12-TMP	5.5±0.6	1282±185	3.4±0.6
PEG2k-AT6-P	11.0±0.6	1573±63	3.8±0.2
PEG2k-AT6-P(DMF)	0.6±0.1	47±5	7.4±0.4
PEG2k-HDA-P	1.9±0.2	448±34	3.7±0.1
PEG2k-AT6-nD-TMP	2.7±0.5	1330±45	5.1±0.2
PEG1k+4k-AT6-TMP	2.4±0.1	1682±24	1.8±0.2

Table 3

Conductivity and mechanical properties of copolymer blends

Filler	Conductivity (S/cm)	Strength (MPa)	Strain (%)	Modulus (MPa)
None	8.2×10^{-6}	10.1±0.9	1643±157	4.2±1.2
2%PANI nanofibers	2.1×10^{-4}	8.4±0.4	1644±22.6	3.8±0.4
2% CB	0.6×10^{-4}	8.1±0.3	1211±52.1	5.9±0.3
20% CB	0.10	10.5±0.7	1334±52.4	7.7±0.9